



# Microstructural evolution, phase formation and mechanical properties of multi-component AlCoCrFeNi<sub>x</sub> alloys

Leigang Cao<sup>1</sup> · Xiaohe Wang<sup>1</sup> · Yiming Wang<sup>1</sup> · Leilei Zhang<sup>1</sup> · Yue Yang<sup>1</sup> · Fengbin Liu<sup>1</sup> · Yan Cui<sup>1</sup>

Received: 5 October 2018 / Accepted: 22 August 2019 / Published online: 12 September 2019  
© Springer-Verlag GmbH Germany, part of Springer Nature 2019

## Abstract

Microstructure evolution and mechanical property of the AlCoCrFeNi<sub>x</sub> ( $1.0 \leq x \leq 3.0$ ) high-entropy alloys were investigated in this paper. Nickel element facilitates the formation of the FCC phase from the BCC matrix. Correspondingly, the microstructure changes from dendrite morphology ( $1.0 \leq x \leq 1.5$ ) to eutectic structure ( $x = 2.1$ ) and finally to oriented cellular structure ( $x \geq 2.4$ ). The onset of the structure transition was observed in the AlCoCrFeNi<sub>1.5</sub> alloy with the formation of the ordered B2 single-phase dendrite, resulting in the observed high strength and hardness in comparison to the AlCoCrFeNi alloy. The compressive yield strength and hardness present a general decreasing trend, dropping from 1360 MPa ( $x = 1.5$ ) to 450 MPa ( $x = 3.0$ ) and from 524 HV ( $x = 1.5$ ) to 241 HV ( $x = 3.0$ ), respectively. The equiaxed grain with dendritic morphology in the AlCoCrFeNi and AlCoCrFeNi<sub>1.5</sub> alloys could be attributed to multiple-nucleation and subsequent growth during the solidification process. The thermodynamic properties of the AlCoCrFeNi<sub>x</sub> ( $1.0 \leq x \leq 1.8$ ) were also studied by DTA measurement, indicating the decreasing fraction of the metastable phase in the as-cast alloys as the Ni content is increased.

## 1 Introduction

High-entropy alloys (HEAs), as a new type of metallic alloys, have been paid great attention for their potential application as high-temperature structural materials due to their high hardness [1–3], wear resistance [4, 5], high-temperature softening resistance [6], good oxidation resistance [7], excellent irradiation resistance [8] and their feasibility of preparation by the conventional casting method [9]. In general, HEAs consists of more than five metallic elements, each ranging from 5 to 35 at.% [10, 11]. However, they tend to form the simple solid solution structures such as BCC, FCC or a mixture of BCC and FCC, rather than complex intermetallic compounds. With this unusual phase formation phenomenon, alloying effect on the microstructures and properties of the HEAs has become one of the most interesting fields so far to reveal the solidification behavior, phase selection and relevant mechanical properties in this multi-component alloy system.

The multiprincipal-element character of HEAs leads to the so-called “core effects”, including high entropy, sluggish

diffusion, severe lattice distortion and cocktail effects [12]. Among these effects, sluggish diffusion effect is very important, acting as the rate-limiting factor for the transformation. First, the processes of the nucleation, grain growth and thereby grain-boundary migration, requiring the redistribution of all elements to reach the desired composition, could be retarded. Second, atomic diffusion ability would be more difficult in the solid state during the subsequent cooling process after liquid–solid phase transformation, resulting in the suppression of the potential solid–solid phase transformation, which could be in favor of the metastable phase in the as-solidified alloys. Initially, sluggish diffusion in the HEAs was postulated based on the model of the atomic level variation of the individual jump barriers induced by the mixture of different elements [13], which was subsequently supported by a large number of investigations [14–17]. However, the majority of recent studies provide solid arguments against this premise [18, 19], indicating that the sluggish diffusion, not an intrinsic characteristic for all of the multi-component alloy systems, is closely related to the alloy composition as it influences the vacancy migration energy directly. Recently, Chen et al. [20] have extended the study to the atomic relaxation processes in high-entropy glass-forming metallic melts and then revealed that the atomic diffusion persists not only in the solid, but also in the liquid states of high-entropy alloy systems. Therefore, one

✉ Yan Cui  
cuiyan@ncut.edu.cn

<sup>1</sup> Department of Materials Science and Engineering, North China University of Technology, Beijing 100144, China

pertinent comment could be that the sluggish diffusion effect does exist in the multi-component HEAs, which is strongly affected by varying the elemental composition.

The Al–Co–Cr–Fe–Ni alloy system is a well-known high-entropy alloy system. Phase constituent of the  $\text{Al}_x\text{CoCrFeNi}$  alloy system is sensitive to the aluminum element, the crystal structure of which could change from FCC, via a mixture of FCC and BCC, to fully BCC with increasing Al content [21]. Correspondingly, a complex microstructural evolution was observed, being from columnar cellular structure, via columnar dendrite structure, equiaxed non-dendritic grain and equiaxed dendritic grain to non-equiaxed dendritic grain structures. A number of studies [2, 3, 21–23] on the same alloy system with the molar ratio,  $x$ , being in the range of 0–3.0, although mainly focusing on other research purposes, also presented the same phase constituent and similar microstructure. The as-cast  $\text{AlCoCrFeNi}$  alloy, being analyzed most thoroughly, consisted of Ni and Al-rich dendritic and Cr and Fe-rich interdendritic regions, both of which presented a nano-scaled microstructure [24]. TEM analysis confirmed that the dendritic microstructure consisted of a B2 matrix and BCC precipitates, while, the interdendritic microstructure consisted of a BCC matrix and B2 precipitates [24–26]. DTA analysis on the  $\text{Al}_x\text{CoCrFeNi}$  alloys by Wang et al. [6] revealed two phase-transition behaviors at about 870 K and 1203–1235 K, corresponding to the disorder  $\text{BCC} \rightarrow \text{FCC} + \sigma$  transformation and the dissolution of  $\sigma$  phase. The presence of the disordered BCC phase, equilibrium phase at high temperature [27], could be attributed to the slow diffusion kinetics [28]. In addition, the influences of Fe content on the microstructure and properties of the  $\text{AlCoCrFe}_x\text{Ni}$  ( $0.2 \leq x \leq 2.0$ ) high-entropy alloys were investigated by Lu et al. [29], wherein the dendritic structure was only observed in the  $\text{AlCoCrFe}_{0.2}\text{Ni}$  alloy and all of the rest alloys presents equiaxed grains morphology. Phase composition changed from  $\text{Cr}_3\text{Ni}_2 + \text{B}_2 + \text{BCC}$  structure to  $\text{B}_2 + \text{BCC}$  mixed structure for Fe content,  $x$ , in excess of 0.6.

Recently Lu et al. [9] have extended their studies to the  $\text{AlCoCrFeNi}$  high-entropy alloy system with high Ni content to improve its comprehensive mechanical property. With the strategy of the eutectic alloy design, they successfully for the first time fabricated a eutectic high-entropy alloy,  $\text{AlCoCrFeNi}_{2.1}$ , comprising alternating soft FCC and hard B2 phases with excellent mechanical properties (high fracture strength and high ductility). Thereafter, eutectic structure was found in many other alloy systems [30–33]. The eutectic structure was only reported in the  $\text{AlCoCrFeNi}_x$  alloys ( $x = 2.0$ – $2.2$  [34]) for the Al–Co–Cr–Fe–Ni five-component alloy system so far. The results indicate that Ni element gives rise to significant transition from dendritic morphology with a BCC and B2 dual-phase structure ( $x = 1.0$ ) to typical eutectic morphology with FCC and B2 structure ( $x = 2.1$ ). However, although it has been indicated that the

microstructure could be affected by the atomic diffusion condition, which is related to the composition of the constitutional element, the effect of Ni content on the solidification behavior of the  $\text{AlCoCrFeNi}_x$  alloy, especially for microstructural evolution ( $1.0 < x < 2.1$ ), is still unclear. Meanwhile, varying the content of Ni is equal to changing the content of Al, which also plays an important role in controlling the microstructure and property of the Al–Co–Cr–Fe–Ni alloy system. The difference is that varying the content of Ni, instead of Al, can reduce the changing interval of the atomic size difference of the alloys, which might be more favorable to investigate the microstructure evolution. Therefore, in this study, as-cast  $\text{AlCoCrFeNi}_x$  high-entropy alloys were prepared using copper mould casting method to study its microstructure evolution involving with typical eutectic structure with increasing Ni content. Mechanical properties of the alloys and solidification behavior of the constituting element were also investigated.

## 2 Experimental details

The multi-principal-element  $\text{AlCoCrFeNi}_x$  high-entropy alloy system with different nickel contents (i.e.,  $x$  values in molar ratio, from 1.0 to 3.0) were prepared by arc-melting the elemental constituents (purity = 99.99% for all of the metals) in a water-cooled copper hearth under a protective argon atmosphere. These alloys were denoted as  $\text{Ni}_x$  for short, e.g., when  $x = 1.5$ ,  $\text{AlCoCrFeNi}_{1.5}$  was denoted as  $\text{Ni}_{1.5}$  in the present paper. Pure titanium ingot was melted first to further remove the residual oxygen in the evacuated chamber. The arc-melting process was repeated five times to ensure uniform mixing of the final samples. The prepared button-shaped ingots ( $\approx 30$  g) had shiny surfaces, indicating that there was no oxidation during the arc-melting process. Single roll melt-spinner allowing the free exchange between the spinning wheel and 2-part copper mould was used to fabricate the casting rods. Cylindrical alloy rods with diameter of  $\varnothing 5 \times 50$  mm were then prepared from the arc-melted ingots in an argon atmosphere by injection copper mold casting. Full details of the sample fabricating process have been published previously [35].

The alloy specimens were then hot-mounted using conductive powder filled with copper to observe the microstructure and measure the phase composition. The mounted samples were ground flat using a series of progressively finer SiC papers, starting with 180, 400, 800, 1000, 1500 and lastly 2000 grit, with optical microscopy being used to check the quality of the surface finish at each stage. Once the samples were appropriately ground they were polished using 6  $\mu\text{m}$ , 3  $\mu\text{m}$ , 1  $\mu\text{m}$  and 0.5  $\mu\text{m}$  diamond paste. The samples were washed using dilute detergent and absolute ethanol and then dried using hot air between each polishing step.

Phase identification was undertaken on non-mounted alloy samples (ground with 2000 grit SiC paper) by X-ray diffraction using a Rigaku Ultimate-IV diffractometer with  $\text{CuK}_\alpha$  radiation. The composition of the well-polished samples was characterized using EDX detection mounted on a Zeiss sigma 300 SEM. Here, BSE detector was also used to assist EDX analysis by pinpointing on the measured area/phase. We note that the size of the identified phase varies in the alloys with different composition, therefore, for EDX analysis, area scan model was chosen to determine the average composition of the large grains, while, for the small grains, point scan was chosen for measurement. As for the reason that point analysis may not be accurate enough if the size of the identified phase is smaller than some microns, point analysis was carried out very carefully by choosing the size of the phase being no less than 5 microns, which was proved to be a reliable measurement in our previous work [36]. Vickers hardness measurement was carried out on polished samples using a TEST-TECH THUS-250 macro-hardness tester at ambient condition (operated at 30 kgf for indentation time of 10 s). Each measurement was repeated a minimum of eight times. The size of the samples for compressive mechanical property test was  $\varnothing 5 \times 10$  mm with a strain rate of  $1 \times 10^{-3} \text{ s}^{-1}$  at room temperature. The TEM disk-shaped foil (5 mm in diameter) was mechanically ground to about 30  $\mu\text{m}$  in thickness, followed by ion milling using a Gatan 691 precision ion polishing system. The TEM examination was then performed using an FEI Tecnai G2 F30 FEG-TEM. DTA measurement was performed under a protective argon atmosphere using a Hitachi STA7300 instrument, which was used to determine the existence of the metastable phase in the as-solidified alloys.

### 3 Results and discussion

#### 3.1 XRD analysis

Figure 1 shows the XRD patterns for the  $\text{AlCoCrFeNi}_x$  alloys ( $x = 1.0, 1.5, 1.8, 2.1, 2.4, 2.7, 3.0$ ) solidified in the copper mould. It is clear that the Ni1.0 alloy presents a simple body-centered-cubic (BCC) crystal structure, which is consistent with the observations as reported elsewhere [22, 37, 38]. With the increasing concentration of Ni element, a face-centered-cubic (FCC) phase forms from the solid-solution matrix alloy. The characteristic peaks of all the diffraction patterns at about  $43.5^\circ$  ( $2\theta$ ) and  $44.3^\circ$  ( $2\theta$ ) correspond to the (111) plane of the FCC phase and the (110) plane of the BCC phase, respectively. The lattice constants of the FCC and BCC solid solution phases are calculated to be about 3.6004  $\text{\AA}$  and 2.8892  $\text{\AA}$ , respectively. When  $x \geq 1.5$ , the relative peak intensities of the FCC phase, in comparison with that of the BCC phase, are increased as the Ni element

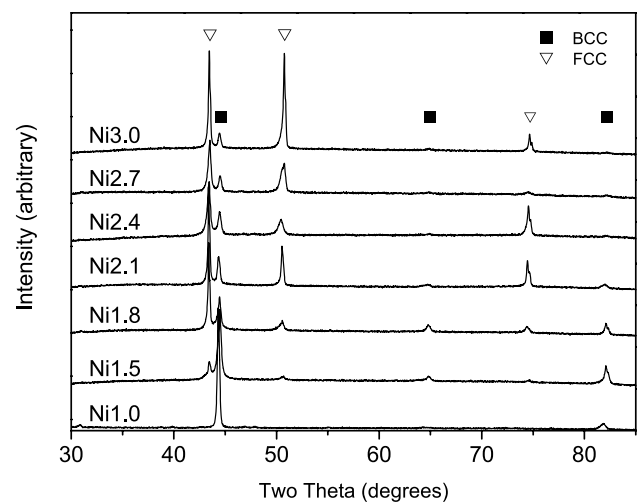


**Fig. 1** XRD results from the  $\text{AlCoCrFeNi}_x$  alloy rods with the diameter of 5 mm, indicating the increasing volume fraction of the FCC phase as the Ni content is increased

is increased, indicating an increasing fraction of the FCC phase in the  $\text{AlCoCrFeNi}_x$  alloy.

Here, some comments relating to the phases present may be pertinent. First, it has been identified that the as-cast  $\text{AlCoCrFeNi}$  alloy consisted of Ni–Al-rich dendritic region with BCC precipitates in the B2 matrix and Cr–Fe-rich interdendritic region with B2 precipitates in the BCC matrix [24–26, 39]. Second, the  $\text{AlCoCrFeNi}_{2.1}$  alloy presents a FCC + B2 eutectic structure. According to our ongoing investigations, the onset of the phase transition was observed in the Ni1.5 alloy, with the formation of the single B2 phase. Therefore, the subsequent statement and discussion related to the phase constitution refer to the facts that the Ni1.0 alloy contains BCC and B2 phases, the Ni1.5 alloys contains BCC, B2 and FCC phases and the rest of alloys ( $x \geq 1.8$ ) mainly contains FCC and B2 phases.

#### 3.2 Microstructure

Both of Ni1.0 and Ni1.5 alloys present typical dendrite morphology (Fig. 2), which is consistent with the observations by Manzoni et al. [25] on the  $\text{AlCoCrFeNi}$  alloy with the grain size being about 1 mm in length. Figure 2a was obtained using the Inlense detector mounted on a Carl Zeiss sigma-300 SEM, resulting in the black spot in the center at lower magnification, which was then covered by another image with high magnification. As can be seen in Fig. 2d (high magnification), for the Ni1.5 alloy, the thin/needle phase formed from the grain boundaries and grew into the grains and the interdendritic region also solidified into dual-phase structure. This new phase is confirmed to be FCC phase according to the XRD analysis. In the Ni1.8 alloy, the dendrite of the B2 phase (dark) was embedded



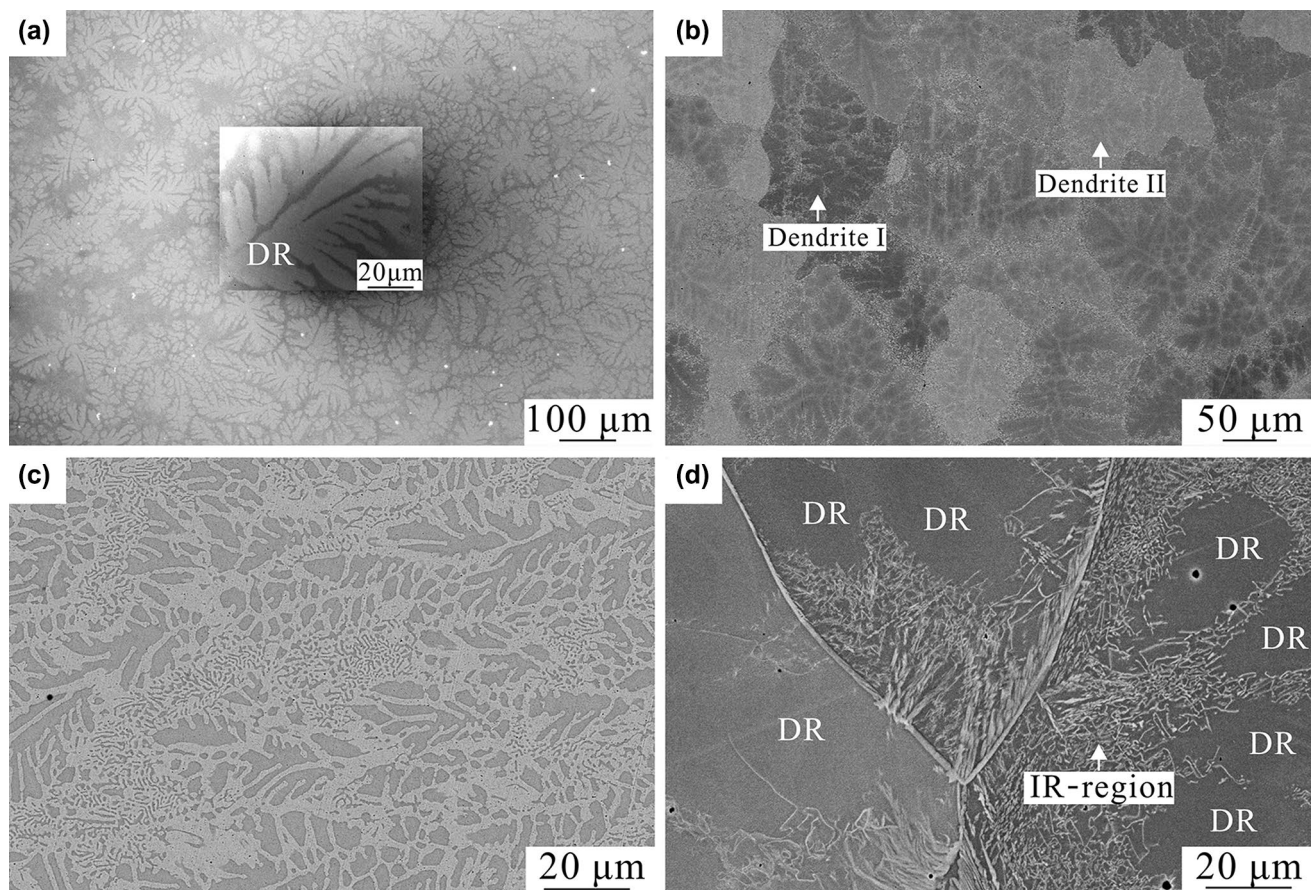


**Fig. 2** a–c SEM micrographs of the Ni1.0, Ni1.5 and Ni1.8 casting rods, respectively, showing the typical dendritic (DR) morphologies. **d** Dendritic structure in **b** at higher magnification showing needle-

like FCC phase at grain boundary and refined dual-phase structure in the interdendritic (IR) region

by the FCC phase (bright), with refined dual-phase structure solidified in the rest region (Fig. 2c).

Instead, the Ni2.1 alloy presents a typical eutectic structure (Fig. 3a) of alternating FCC and B2 lamellae, which is consistent with the reported observations [9, 40–42]. The refined microstructure, different from the structure observed in the other alloys in the present paper, is due to the distinct eutectic growth mechanism. During lamellar eutectic growth, the dominant diffusion direction should be fairly perpendicular to the solidification direction which will reduce the solute accumulation ahead of both phases [43]. That is, the FCC phase will reject Al and Ni atoms into the melt, while the B2 phase will reject the other three kinds of atoms. Since the FCC and B2 phases are placed side-by-side, Al and Ni atoms rejected by FCC phase are in favor of the growth of the B2 phase, and Co, Cr, and Fe atoms rejected by B2 phase are in favor of the growth of the FCC phase. Sideways diffusion could accelerate the solidification rate and is also the reason to form alternative refined lamellae of FCC and B2 phases, which indicated

the availability of the atomic mobility in the liquid–solid transition process of multi-component alloy system.

The cellular growth of the FCC phase occurs in the AlCoCrFeNi<sub>x</sub> alloys with *x* in excess of 2.4, as shown in Fig. 3b–d. It is obvious that the fraction of eutectic region is much lower than that of the primary solidified FCC phase. With the increasing trend of the volume fraction of FCC phase, we can speculate that the AlCoCrFeNi<sub>x</sub> alloys could possess single FCC crystal structure when the Ni composition exceeds a certain value ( $x > 3$ ).

### 3.3 EDX analysis

EDX measurement was carried out to check the average elemental compositions of the alloys. For the Ni1.0 alloy, only the average composition of the dendrite was measured. Since the dendrite structure in Ni1.5 alloy presents different contrasts under backscatter detector, light colour (dendrite I) and dark colour (dendrite II), the corresponding EDX measurement was performed separately, the results of which



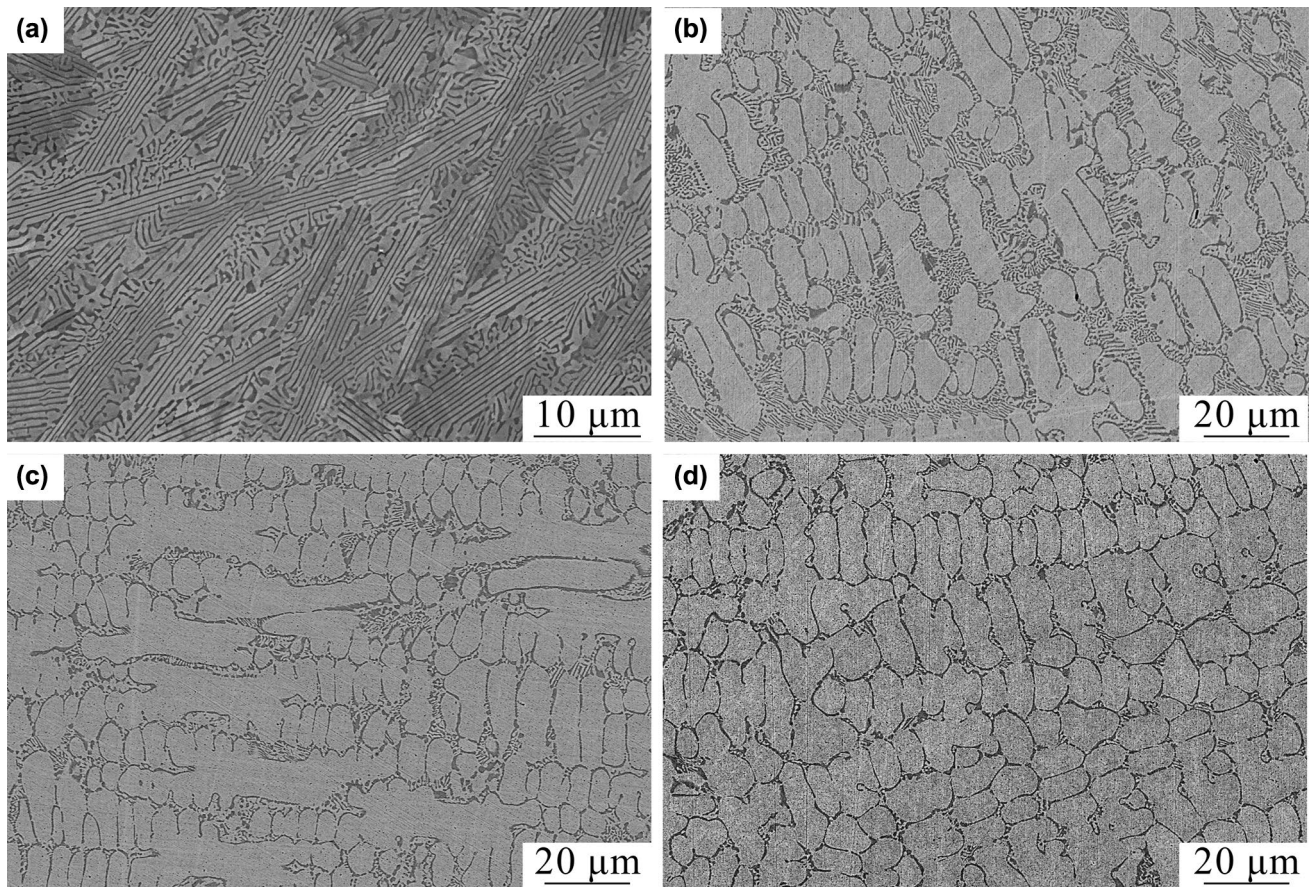


**Fig. 3** SEM micrographs of the AlCoCrFeNi<sub>x</sub> ( $x \geq 2.1$ ) alloy rods. **a** Ni2.1, presenting a typical eutectic structure; **b** Ni2.4 **c** Ni2.7 and **d** Ni3.0, showing the typical hyper-eutectic morphology

**Table 1** The EDX results of the dendrite for the Ni1.0 and Ni1.5 alloys

Alloy	Al/at.%	Co/at.%	Cr/at.%	Fe/at.%	Ni/at.%
Ni 1.0					
Nominal	20.00	20.00	20.00	20.00	20.00
Dendrite	22.77 ± 1.75	20.45 ± 0.28	17.85 ± 1.61	19.07 ± 1.01	19.94 ± 0.91
Ni 1.5					
Nominal	18.18	18.18	18.18	18.18	27.27
Dendrite I	24.34 ± 0.53	17.98 ± 0.21	13.32 ± 0.33	15.73 ± 0.35	28.63 ± 0.41
Dendrite II	20.88 ± 0.32	18.43 ± 0.18	16.11 ± 0.70	17.27 ± 0.29	27.32 ± 0.65

are shown in Table 1. The Al compositions of dendrite I and II are 24.34 at.% and 20.88 at.%, respectively, which is the main reason for the contrast difference since the atomic numbers of Ni, Co, Fe and Ni are quite close.

The average elemental compositions of the B2 and FCC phases in the AlCoCrFeNi<sub>x</sub> ( $x \geq 1.8$ ) alloys were also measured using EDX, as shown in Table 2. For each alloy, point/area scans on at least ten random grains were performed to determine the average composition. Several important observations can be made according to the EDX results of the HEAs with the increasing Ni composition.

First, the B2 phase has higher compositions of the Ni and Al elements, while the FCC phase has higher compositions of Co, Cr and Fe elements in comparison with the nominal elemental composition of the corresponding alloys. Second, Ni composition of both BCC and FCC phases in AlCoCrFeNi<sub>x</sub> alloys presents the same increasing trend as the Ni composition of the alloys is increased. For the B2 phase, Ni composition increases from 31.82 at.% (Ni1.8 alloy) to 45.05 at.% (Ni3.0 alloy), while, for the FCC phase, Ni composition increases from 28.61 at.% (Ni1.8 alloy) to 40.55 at.% (Ni3.0 alloy).

**Table 2** The EDX results of the phases for the Ni1.8, Ni2.1, Ni2.4, Ni2.7, and Ni3.0 alloys

Alloy	Al/at.%	Co/at.%	Cr/at.%	Fe/at.%	Ni/at.%
Ni 1.8					
Nominal	17.24	17.24	17.24	17.24	31.03
B2 phase	21.65 ± 0.56	16.52 ± 0.31	14.23 ± 0.39	15.73 ± 0.32	31.82 ± 0.54
FCC phase	12.73 ± 0.48	18.96 ± 0.57	19.97 ± 0.53	19.73 ± 0.57	28.61 ± 0.55
Ni 2.1					
Nominal	16.39	16.39	16.39	16.39	34.43
B2 phase	25.07 ± 0.83	13.95 ± 0.42	11.76 ± 0.44	12.54 ± 0.51	36.69 ± 0.74
FCC phase	15.02 ± 0.60	17.59 ± 0.27	18.00 ± 0.65	17.95 ± 0.29	31.45 ± 0.25
Ni 2.4					
Nominal	15.63	15.63	15.63	15.63	37.50
B2 phase	27.69 ± 0.64	12.05 ± 0.27	9.40 ± 0.31	10.68 ± 0.27	40.18 ± 0.53
FCC phase	13.18 ± 0.40	17.74 ± 0.22	16.16 ± 0.23	17.77 ± 0.12	35.15 ± 0.29
Ni 2.7					
Nominal	14.93	14.93	14.93	14.93	40.30
B2 phase	27.13 ± 0.72	10.80 ± 0.36	9.42 ± 0.58	10.00 ± 0.39	42.64 ± 0.58
FCC phase	12.85 ± 0.30	16.80 ± 0.20	15.23 ± 0.25	16.92 ± 0.21	38.20 ± 0.37
Ni 3.0					
Nominal	14.29	14.29	14.29	14.29	42.86
B2 phase	27.86 ± 0.72	9.53 ± 0.19	8.58 ± 0.33	8.98 ± 0.22	45.05 ± 0.43
FCC phase	12.87 ± 0.22	15.86 ± 0.23	14.81 ± 0.20	15.91 ± 0.26	40.55 ± 0.37

However, Al composition did not present the same trend. For the Ni 1.8 alloy (17.24 at.% Al), the Al composition in the FCC phase is about 12.73 at.%, which increases to about 15.02 at.% for the eutectic Ni2.1 alloy (16.39 at.% Al). Then, the average Al composition of the FCC phase in the Ni2.4 (15.63 at.% Al), Ni2.7 (14.93 at.% Al), Ni3.0 (14.29 at.% Al) alloys, irrespective of the Ni content, decreases to a relative stable level, being about 13.18 at.%, 12.85 at.% and 12.87 at.%, respectively. High Al composition of the FCC phase in Ni2.1 alloy would be because of the distinct eutectic growth mechanism.

Meanwhile, the average Al composition of the B2 phase in Ni1.8 alloys is 21.65 at.%, which increases to 25.07 at.%, 27.69 at.%, 27.13 at.% and 27.86 at.% for the Ni2.1, Ni2.4, Ni2.7 and Ni3.0 alloys, respectively. In addition, the compositions of Co, Cr, and Fe atoms for both B2 and FCC phases decrease gradually with increasing Ni composition of the corresponding alloys.

### 3.4 Mechanical property

Figure 4 shows the compressive stress–strain curves of AlCoCrFeNi<sub>x</sub> alloys with different Ni contents at the strain rate of  $1.0 \times 10^{-3} \text{ mm s}^{-1}$ . The compressive strengths of all alloys are higher than 2380 MPa, except for the Ni2.1 alloy, which was finally compressed into a drum shape. The yield stress, fracture strength and plastic strain limits are given in Table 3. The yield stress ( $\sigma_y$ ) of the Ni1.0 alloy was about 1350 MPa, which increases slightly to 1360 MPa for the Ni1.5 alloy and then drops sharply to 600 MPa for the Ni1.8 alloy. The yield stress increases again to 670 MPa for the Ni2.1 eutectic alloy and then decreases gradually to 450 MPa for the Ni3.0 alloy. The results of the Ni1.0 and Ni2.1 alloys are broadly in line with the measurements by Zhou et al. [44] and Lu et al. [34], respectively (Table 3).

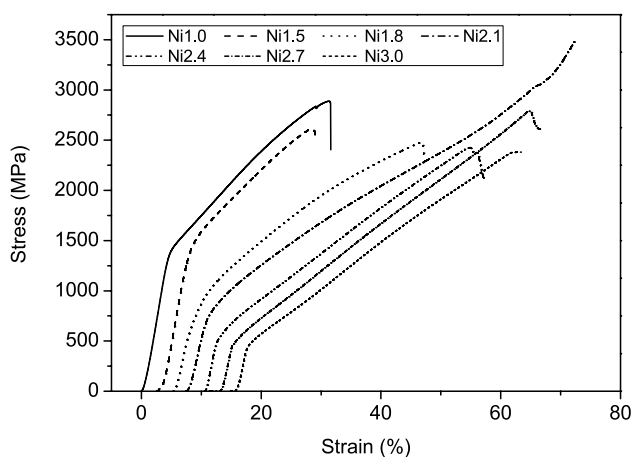


**Fig. 4** Engineering compressive stress–strain curves for the AlCoCrFeNi<sub>x</sub> alloy rods with diameter of 5 mm at room temperature

**Table 3** The results of the mechanical properties according to Fig. 5 and several other references

Alloy	$\sigma_y$ (MPa)	$\sigma_{\max}$ (MPa)	Strain, $\epsilon_p$ (%)	References
Ni 1.0	1350	2840	24.2	This work
	1500	2830	26.9	[29]
	1423	2582	22.7	[19]
Ni 1.5	1360	2610	20.8	This work
Ni 1.8	600	2470	37.6	This work
Ni 2.1	670	–	–	This work
	545	1100	16–17	[30]
Ni 2.4	500	2430	42.5	This work
Ni 2.7	470	2790	49.3	This work
Ni 3.0	440	2380	44.7	This work

Yield stress ( $\sigma_y$ ), fracture strength ( $\sigma_{\max}$ ) and plastic strain ( $\epsilon_p$ )

All of the data were taken from the compressive testing of the casting rod ( $\Phi 5 \times 10 \text{ mm}$ ), except for [30], which were from tensile testing

Correspondingly, the plastic strain ( $\epsilon_p$ ) of the alloys with high Ni content ( $x \geq 2.4 \text{ at.}\%$ ) was higher than 40%, in comparison to that of the Ni1.0 and Ni1.5 alloys. As can be seen in Fig. 5, the hardness of the alloys follows a more simple trend that the average hardness increases slightly from 488 HV (Ni1.0 alloy) to 524 HV (Ni1.5 alloy) and then drops to 241 HV (Ni3.0) gradually. Here, the decrease of the yield compressive strength and hardness and the increase of plastic strain could be attributed to the increasing fraction of the “soft” FCC phase with increasing Ni content, since the BCC phase is much stronger than the FCC phase [45]. Similar results were also reported in the studies on AlCoCrCuFeNi alloy system [2, 11, 45].

One common feature here for both Ni1.0 and Ni1.5 alloys is the formation of the large grains with dendrite structure

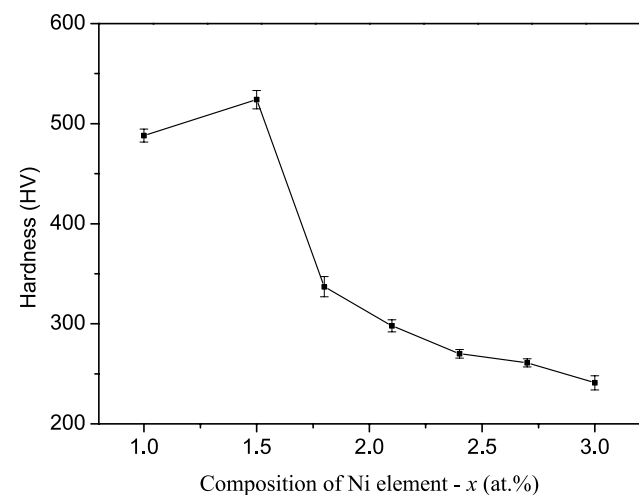


**Fig. 5** Hardness measurement of the AlCoCrFeNi<sub>x</sub> alloy rods as a function of the Ni content



inside. It has been well accepted that both dendrite and interdendrite of the AlCoCrFeNi (Ni1.0) alloy consist of nano-scale two-phase microstructure [6, 21, 25]. Therefore, to study the microstructure evolution as the Ni content is increased, TEM detection was carried out to reveal the microstructure of the Ni1.5 alloy, the results of which are shown in Fig. 6. This shows a nano-scale dual-phase structure (Fig. 6a), as was reported in the Ni1.0 alloy. More importantly, TEM detection reveals a dual-phase structure and a large single phase (Fig. 6b). A selected-area diffraction pattern confirms that this single-phase region and therefore the phase (light grey) of the mixture structure are the ordered B2 phase. The other phase should be the FCC phase according to the XRD analysis (inset of Fig. 6b). According to the EDS analysis and the SEM image in Fig. 2b, d, the microstructure of Fig. 6a, b refers to the areas of the dendrite I and dendrite II. That is to say, in the Ni1.5 alloy, the dendrite regions are either single-phase B2 (Fig. 6b) or the nano-scale mixture microstructure (Fig. 6a), while the interdendrite region consists of FCC and B2 phases, which is consistent with the refined structure presented in Fig. 2d. According to

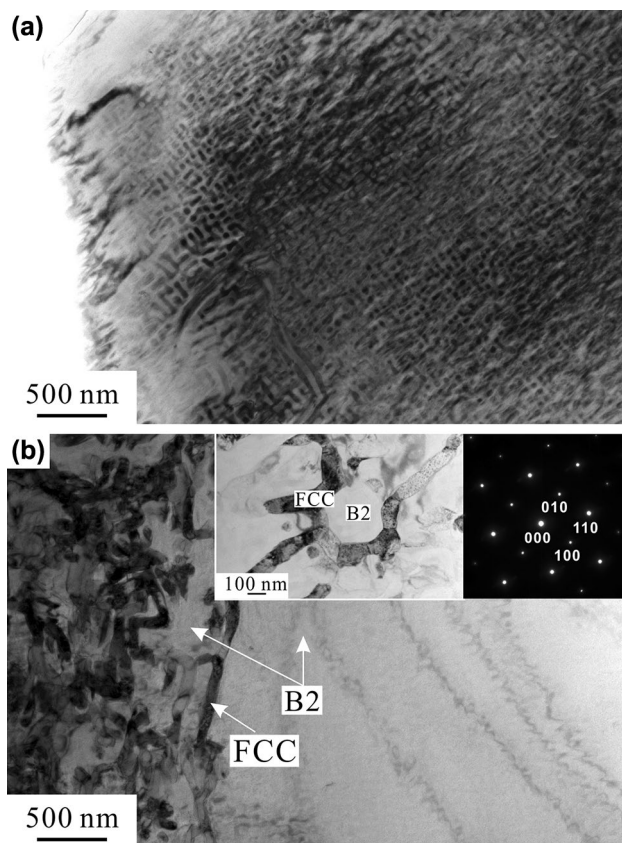


**Fig. 6** **a** TEM micrographs of the dendrite I in Ni1.5 alloy, presenting a nano-scale mixture microstructure and **b** TEM micrographs of the dendrite II, indicating the formation of the large-scale, ordered B2 single phase. The interdendrite region consists of FCC and B2 phases

EDX analysis, Al composition of the dendrite II (light colour 20.88 at.%) for the Ni1.5 alloy is only slightly lower than that of the dendrite (22.77 at.%) for the Ni1.0 alloy. Such a high composition of Al content would give rise to serious lattice distortion and then strengthen the mechanical property. This could be the reason that, although the “soft” FCC phase formed in the interdendrite region of the Ni1.5 alloy, the alloy still presents high compressive yield strength and hardness. Therefore, the enhanced lattice distortion would be the dominant reason for the fact that compressive yield strength and hardness of the Ni1.5 alloy are slightly higher than that of the Ni1.0 alloy. The subsequent drop of the mechanical property could be attributed to the increasing fraction of the FCC phase with increasing Ni content. In addition, the increasing yield compressive strength of the Ni2.1 alloy is attributed to the refined eutectic microstructure in comparison to that of the Ni1.8 alloy.

### 3.5 DTA analysis

To reveal the phase stability of the as-solidified HEAs, DTA analysis was performed on the Ni1.0, Ni1.5 and Ni1.8 alloys

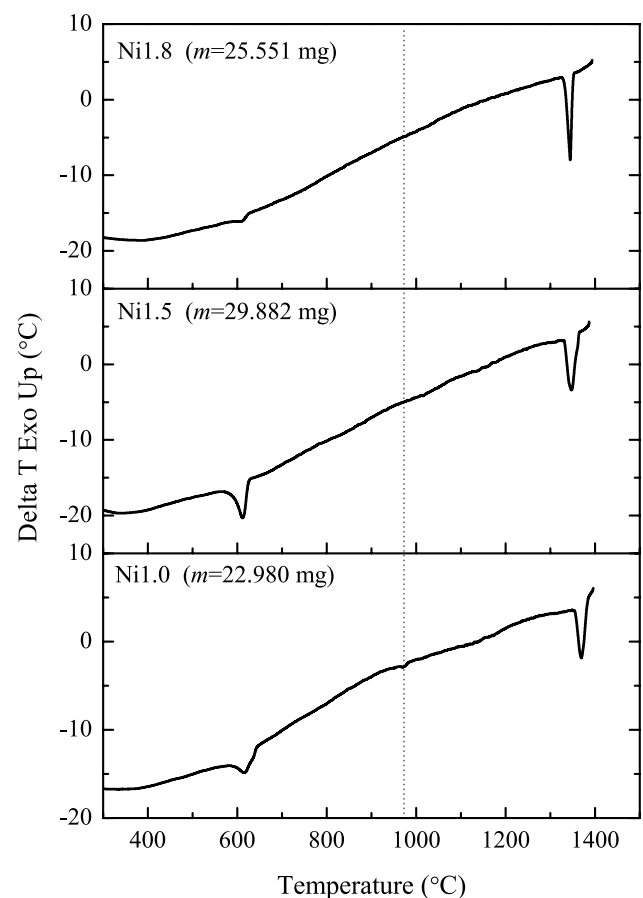


**Fig. 7** DTA curves of the Ni1.0, Ni1.5 and Ni1.8 alloys with the heating rate being  $10 \text{ K min}^{-1}$



with heating rate of  $10 \text{ K min}^{-1}$ , the results of which are shown in Fig. 7. According to previous studies [6, 24], the first endothermic peaks near  $600 \text{ }^\circ\text{C}$  for all of the samples is ascribed to the phase transformation of the disordered BCC phase. The weak endothermic peak near  $970 \text{ }^\circ\text{C}$  for the Ni1.0 alloy is related to the dissolution of  $\sigma$  phase, the absence of which in the heating curves of the Ni1.5 and Ni1.8 alloys is probably due to the low fraction of the decomposed  $\sigma$  phase. The exothermic peak at high temperature ( $\approx 1340 \text{ }^\circ\text{C}$ ) corresponds to the melting process of the alloys. As can be seen in Fig. 7, the endothermic peak near  $600 \text{ }^\circ\text{C}$  of the Ni1.8 alloy is weaker than that of the Ni1.0 and Ni1.5 alloys, indicating the fraction of the disordered BCC phase in the as-cast alloys decreases as the Ni content is decreased. This trend is in line with the DTA analysis performed by Lu et al., who revealed that there is no phase transition during the heating process, except for the melting event at high temperature in the eutectic AlCoCrFeNi<sub>2.1</sub> alloy.

#### 4 Further discussion

Phase constitutions in the as-cast HEAs could be considered as the quenched phases (e.g., metastable phase) that are at equilibrium at temperatures closest to the solidus temperature, due to the slow diffusion kinetics in HEAs and the relatively short time scale for the solidification [28]. This makes it possible to modify the microstructure and mechanical properties of the as-solidified HEAs with the precipitation of the second phase by means of heat-treatment method, e.g., FCC precipitates in the annealed CoCrFeNiNb<sub>0.25</sub> alloy [46], nano-sized B2 phase in the heat-treated Al<sub>0.5</sub>CoCrFeNi alloy [47] and precipitations in the heat-treated AlCrFeNi<sub>2</sub>Ti<sub>0.5</sub> [48]. Here, the formation of the disordered BCC phase (equilibrium phase at high temperature [27]) is related to alloy composition and cooling rate during solidification. According to the experimental results described above, we may conclude that the former factor, alloy composition (increasing Ni content), plays an important role in the decreasing fraction of the disordered BCC phase (unstable) and the evolution of the microstructure morphology since the cooling rates of the studied alloys could be treated as the same during solidification of 5 mm casting rod in the copper mould. Although the solidification is expected to be far away from the thermodynamic equilibrium for the studied alloys, the observed phase constitution has strong parallels with theoretical works on AlCoCrFeNi<sub>x</sub> alloys by Zhang et al. [27], who predicted that Ni element can suppress the disordered BCC phase, and stabilize the FCC and ordered B2 phases. According to the previous studies, the formation of the disordered BCC phase, irrespective of the fabricating process and the sample size, has been observed in the AlCoCrFeNi alloy, such

as arc-melted button sample of  $\Phi 37 \text{ mm} \times 11 \text{ mm}$  [24] and of  $45 \text{ mm} \times 45 \text{ mm} \times 10 \text{ mm}$  [21], and casting sample of  $10 \text{ mm} \times 10 \text{ mm} \times 60 \text{ mm}$  [49]. Therefore, it seems to be that, in the current experimental condition, cooling rate is not the main factor for formation of the disordered BCC phase.

As discussed above, sluggish diffusion effect could be strongly affected by varying the composition of the constitutional element, giving rise to the microstructural evolution. The observations in the present study are consistent with the comment. First, atomic size difference ( $\delta$ ), is one of the rough evaluation parameters for atomic diffusion ability [28, 29]. The calculated results are given in Table 4 based on the atomic radii of the pure elements [29, 37] for understanding the liquid–solid solidification. Significant differences in atomic size ratios can lead to the sluggish diffusion of atoms in the multi-component alloy system. Therefore, where the equiaxed grains with dendritic morphology in the Ni1.0 and Ni1.5 alloys, independent of the heat release direction, this could be attributed to the multiple nucleation mechanism. It could be possible because multiple nucleation might be favoured if the liquids (Ni1.0 and Ni1.5 alloys) experience high undercooling prior to solidification with the consideration of sluggish diffusion, thereby activating more nuclei in the undercooled melt. Second, the difference of the elemental composition of the grains in Fig. 2b also indicates the slow atomic diffusion and thereby a fairly straightforward picture may be put forward. Composition fluctuation might occur in the liquid as the temperature is decreasing prior to solidification, namely that the liquid could be segregated into a number of “zones” with different elemental composition, followed by the dendritic growth of the solid with different crystal structure. For example, the grains in the Ni1.5 alloy presented a variation in contrast using the backscatter detector, with the typical observations of dendrite I (light color) and dendrite II (dark color) in Fig. 2b. The feature was also observed in the other HEAs [50, 51]. The nano-scaled microstructure observed in the dendrite I (24.34 at.% Al) is attributed to the dendritic growth, followed by a spinodal decomposition [24, 25]. As can be seen in Fig. 6b, the regular structure presented in dendrite II (20.88 at.% Al) seems superficially to be as expected from the hypoeutectic alloy, with single-phase regions and a eutectic. TEM analysis

**Table 4** The calculated atomic size differences ( $\delta$ ) of the AlCoCrFeNi<sub>x</sub> alloys

Alloys	$\delta/\%$
Ni1.0	5.78
Ni1.5	5.59
Ni1.8	5.48
Ni2.1	5.38
Ni2.4	5.28
Ni2.7	5.19
Ni3.0	5.10

confirms that the single-phase regions and one of the phases in the eutectic are B2. According to the XRD analysis, the other phase in the eutectic should be the FCC phase. This is consistent with phase constituent of the AlCoCrFeNi<sub>2.1</sub> eutectic alloy [9, 27]. Third, large amounts of Ni element can decrease the atomic size differences,  $\delta$ . Accordingly, with increasing Ni content the microstructure of the Ni1.8, Ni2.4, Ni2.7 and Ni3.0 alloys presents a preferential orientation being opposite to the heat flow direction. This might be due to the relieved sluggish diffusion and improved atomic mobility caused by the decreasing atomic size difference (Table 4).

Recently, Chen et al. [52] has studied the impact of lattice distortion on solid solution strengthening in HEAs. With the consideration of the actual environment of the atoms in the solid (rather than the liquid), they recalculated the atomic radii of the alloying elements on the basis of the mean atomic radii in and the chemical compositions of the solid solutions for the more accurate  $\delta$  values. A quite different result about the atomic radius was revealed, namely that the recalculated radius of Al (1.3172 Å) in the BCC crystal structure of the Nb–Mo–Cr–Ti–Al system is smaller than that of the pure element (1.4317 Å). Therefore, the severe lattice distortion could be expected in the solid phase and, by analogy, in the alloys presented here, especially for the AlCoCrFeNi<sub>x</sub> alloys with low Ni content. Serious lattice distortion would give rise to the difficulty of atomic diffusion in the solid, thereby resulting in a low solid-state phase transformation rate during the subsequent cooling period [53], such as the disorder-order transition. It is consistent with the description that large amounts of Ni content (decreasing Al content) can decrease the atomic size difference of the HEAs and, in turn, weaken the lattice distortion of the solid, stabilizing the ordered B2 phase in the as-solidified alloys.

The presence of the eutectic structure in the AlCoCrFeNi<sub>2.1</sub> alloy is not consistent with the prediction of the AlCoCrFeNi<sub>x</sub> alloy system by Zhang et al. [27], who indicate that the eutectic composition for FCC and B2 phases is of  $x \approx 1.53$ . However, there is no clue for eutectic solidification with the microstructure observation of the Ni1.5 alloy. Meanwhile, Lu et al. [34] fabricated a large sample with the same composition (approximately 2.5 kg) using a vacuum induction melting furnace. Although the solidification conditions of this cylindrical alloys of about  $\phi 55 \times 220$  mm [34] and  $\phi 5 \times 50$  mm in this study are expected to be different, with the former experiencing a slow solidification rate (close to the equilibrium condition) and the latter experiencing a rapid solidification rate (far away from the equilibrium condition), both alloys presents a typical eutectic microstructure. The subsequent DTA also failed to indicate the decomposition of the metastable phase in the as-solidified AlCoCrFeNi<sub>2.1</sub> alloy [34]. Therefore, it could be concluded that the AlCoCrFeNi<sub>2.1</sub> alloy is the eutectic composition of

this alloy system, although the eutectic composition might be slightly shifted under the non-equilibrium condition.

For a typical binary eutectic alloy system, the predicated solidification paths of the hypo-eutectic and hyper-eutectic alloy should be similar, namely that the single-phase forms first from the liquid and eutectic solidification occurs subsequently when the remaining liquid in the interdendritic region equals the eutectic composition. This morphology was also observed in the high-entropy alloy system, e.g., CoFeNi<sub>2</sub>V<sub>0.5</sub>Nb<sub>x</sub> [54], which presents hypoeutectic microstructure of primary FCC single-phase and FCC + Laves phase eutectic and hyper-eutectic microstructure of primary Laves phase and FCC + Laves phase eutectic. In the present paper, Ni2.4, Ni2.7 and Ni3.0 alloys present a typical hyper-eutectic structure (primary single phase and eutectic region). However, the alloys with low Ni content did not show the hypo-eutectic structure. As discussed above the asymmetry described here could be attributed to the interplay of atomic diffusion and alloy composition (Ni content).

## 5 Conclusions

Phase composition, microstructure and mechanical properties of AlCoCrFeNi<sub>x</sub> ( $x = 1.0\text{--}3.0$ ) high-entropy alloys were investigated, with the following conclusions being derived from the present work.

1. AlCoCrFeNi alloy presents a simple BCC phase constitution, while an increasing fraction of the FCC phase solidified in the AlCoCrFeNi<sub>x</sub> ( $x \geq 1.5$ ). The Al and Ni elements are enriched in the BCC phase, while the Co, Cr and Fe elements are enriched in the FCC phase.
2. Large amount of Ni element facilitates the microstructure evolution from equiaxed grains with dendrite morphology ( $1.0 \leq x \leq 1.5$ ) to eutectic structure ( $x = 2.1$ ) and finally to oriented cellular structure ( $x \geq 2.4$ ).
3. Compressive yield strengths for the Ni1.0 and Ni1.5 alloys are about 1350 MPa and 1360 MPa, respectively, which drops to 600 MPa for the Ni1.8 alloy. The compressive yield strength increases to 670 MPa for the Ni2.1 alloy and then decreases gradually to 450 MPa for the Ni3.0 alloy with the increase of Ni content. Hardness increases slightly from 488 HV for Ni1.0 alloy to 524 HV for Ni 1.5 alloy and then decreases gradually to 241 HV for the Ni3.0 alloy.
4. The onset of structure transition was observed in the AlCoCrFeNi<sub>1.5</sub> alloy with the formation of the B2 single-phase dendrite, resulting in the high compressive yield strength and hardness, even with the formation of the “soft” FCC phase. The decrease of the mechanical property is attributed to the increasing volume fraction of the “soft” FCC phase as the Ni content is increased.

5. The fraction of the metastable phase decreases as the Ni content is increased, which could be attributed to the enhanced atomic diffusion rate.

**Acknowledgements** This work is financially supported by National Key R&D Program of China (No. 2017YFB0703102), Yuqing Talent support program (18XN012-081) and Research Start-Up Funding of North China University of Technology.

## References

- A. Heczal, M. Kawasaki, J.L. Lábár, J. Jang, T.G. Langdon, J. Gubicza, *J. Alloy. Compd.* **711**, 143 (2017)
- C.M. Lin, H. Tsai, *Intermetallics* **19**, 288 (2011)
- C.J. Tong, M.R. Chen, J.W. Yeh, S.J. Lin, S.K. Chen, T.T. Shun, S.Y. Chang, *Metall. Mater. Trans. A* **36**, 1263 (2005)
- A. Poulia, E. Georgatis, A. Lekatou, A.E. Karantzalis, *Met. Hard. Mater.* **57**, 50 (2016)
- M.H. Chuang, M.H. Tsai, W.R. Wang, S.J. Lin, J.W. Yeh, *Acta Mater.* **59**, 6308 (2011)
- W.R. Wang, W.L. Wang, J.W. Yeh, *Phases. J. Alloy. Compd.* **589**, 143 (2014)
- B. Gorr, M. Azim, H.J. Christ, T. Mueller, D. Schliephake, M. Heilmaier, *J. Alloy. Compd.* **624**, 270 (2015)
- Y. Lu, H. Huang, X. Gao, C. Ren, J. Gao, H. Zhang, S. Zheng, Q. Jin, Y. Zhao, C. Lu, T. Wang, T. Li, *J. Mater. Sci. Technol.* **35**, 369 (2019)
- Y. Lu, Y. Dong, S. Guo, L. Jiang, H. Kang, T. Wang, B. Wen, Z. Wang, J. Jie, Z. Cao, H. Ruan, T. Li, *Sci. Rep.* **4**, 6200 (2014)
- B. Cantor, I.T.H. Chang, P. Knight, A.J.B. Vincent, *Mater. Sci. Eng. A* **375–377**, 213 (2004)
- J.W. Yeh, S.K. Chen, S.J. Lin, J.Y. Gan, T.S. Chin, T.T. Shun, C.H. Tsau, S.Y. Chang, *Adv. Eng. Mater.* **6**, 299 (2004)
- M.H. Tsai, J.W. Yeh, *Mater. Res. Lett.* **2**, 107 (2014)
- J.W. Yeh, *Eur. J. Control.* **31**, 633 (2006)
- K.Y. Tsai, M.H. Tsai, J.W. Yeh, *Acta Mater.* **61**, 4887 (2013)
- Q. Li, W. Chen, J. Zhong, L. Zhang, Q. Chen, Z.K. Liu, *Metals* **8**, 16 (2017)
- R. Wang, W. Chen, J. Zhong, L. Zhang, *J. Mater. Sci. Technol.* **34**, 1791 (2018)
- Y. Tan, J. Li, J. Wang, H. Kou, *Intermetallics* **85**, 74 (2017)
- Y.N. Osetsky, L.K. Béland, A.V. Barashev, Y. Zhang, *Opin. Solid State Mater. Sci.* **22**, 65 (2018)
- S.V. Divinski, A. Pokoev, N. Esakkiraja, A. Paul, *Diffus. Found.* **17**, 69 (2018)
- C. Chen, K. Wong, R.P. Krishnan, J.P. Embs, S.M. Chathoth, *J. Phys. D Appl. Phys.* **51**, 145301 (2018)
- W.R. Wang, W.L. Wang, S.C. Wang, Y.C. Tsai, C.H. Lai, J.W. Yeh, *Intermetallics* **26**, 44 (2012)
- F. Wang, Y. Zhang, G.L. Chen, H.A. Davis, *J. Eng. Mater. Technol.* **131**, 034501 (2009)
- C. Li, J.C. Li, M. Zhao, Q. Jiang, *J. Alloy. Compd.* **504**, S515 (2010)
- A. Munitz, S. Salhov, S. Hayun, N. Frage, *J. Alloy. Compd.* **683**, 221 (2016)
- A. Manzoni, H. Daoud, R. Völkl, U. Glatzel, N. Wanderka, *Ultra-microscopy* **132**, 212 (2013)
- Y.P. Wang, B.S. Li, M.X. Ren, C. Yang, H.Z. Fu, *Mater. Sci. Eng. A* **491**, 154 (2008)
- C. Zhang, F. Zhang, S. Chen, W. Cao, *JOM* **64**, 839 (2012)
- C. Ng, S. Guo, J. Luan, S. Shi, C.T. Liu, *Intermetallics* **31**, 165 (2012)
- Q. Chen, K. Zhou, L. Jiang, Y. Lu, T. Li, *Arab. J. Sci. Eng.* **40**, 3657 (2015)
- K. Zhou, Z. Tang, Y. Lu, T. Wang, H. Wang, T. Li, *J. Mater. Sci. Technol.* **33**, 131 (2017)
- Y. Dong, L. Jiang, H. Jiang, Y. Lu, T. Wang, T. Li, *Mater. Des.* **82**, 91 (2015)
- L. Jiang, Y. Lu, W. Wu, Z. Cao, T. Li, *J. Mater. Sci. Technol.* **32**, 245 (2016)
- X. Jin, Y. Zhou, L. Zhang, X. Du, B. Li, *Mater. Lett.* **216**, 144 (2018)
- Y. Lu, X. Gao, L. Jiang, Z. Chen, T. Wang, J. Jie, H. Kang, Y. Zhang, S. Guo, H. Ruan, Y. Zhao, Z. Cao, T. Li, *Acta Mater.* **124**, 143 (2017)
- B. Karpe, B. Kosec, M. Bizjak, *J. Achiev. Mater. Manuf. Eng.* **51**, 59 (2012)
- L. Cao, R.F. Cochrane, A.M. Mullis, *Intermetallics* **60**, 33 (2015)
- Y. Dong, K. Zhou, Y. Lu, X. Gao, T. Wang, T. Li, *Mater. Des.* **57**, 67 (2014)
- Y. Zhang, S.G. Ma, J.W. Qiao, *Metall. Mater. Trans. A* **43**, 2625 (2011)
- Y. Linden, M. Pinkas, A. Munitz, L. Meshi, *Scr. Mater.* **139**, 49 (2017)
- I.S. Wani, T. Bhattacharjee, S. Sheikh, Y.P. Lu, S. Chatterjee, P.P. Bhattacharjee, *Mater. Res. Lett.* **4**, 174 (2016)
- T. Bhattacharjee, I.S. Wani, S. Sheikh, I.T. Clark, T. Okawa, S. Guo, P.P. Bhattacharjee, N. Tsuji, *Sci. Rep.* **8**, 3276 (2018)
- P. Shi, W. Ren, T. Zheng, Z. Ren, X. Hou, J. Peng, P. Hu, Y. Gao, Y. Zhong, P.K. Liaw, *Nat. Commun.* **10**, 1 (2019)
- K. Fisher, W. Kurz, *Fundamentals of solidification*, 1st edn. (Trans Tech Publications, Zurich, 1986), p. 100
- Y.J. Zhou, Y. Zhang, Y.L. Wang, G.L. Chen, *Appl. Phys. A* **90**, 181904 (2007)
- C.C. Tung, J.W. Yeh, T. Shun, S.K. Chen, Y.S. Huang, H.C. Chen, *Mater. Lett.* **61**, 1 (2007)
- F. He, Z. Wang, S. Niu, Q. Wu, J. Li, J. Wang, C.T. Liu, Y. Dang, *J. Alloy Compd.* **667**, 53 (2016)
- S. Niu, H. Kou, T. Guo, Y. Zhang, J. Wang, J. Li, *Mater. Sci. Eng. A* **671**, 82 (2016)
- L. Jiang, H. Jiang, Y. Lu, T. Wang, Z. Cao, T. Li, *J. Mater. Sci. Technol.* **31**, 397 (2015)
- J.Y. He, W.H. Liu, H. Wang, Y. Wu, X.J. Liu, T.G. Nieh, Z.P. Lu, *Acta Mater.* **62**, 105 (2014)
- N.D. Stepanov, N.Y. Yurchenko, S.V. Zhrebtsov, M.A. Tikhonovsky, G.A. Salishchev, *Mater. Lett.* **211**, 87 (2017)
- G.A. Salishchev, M.A. Tikhonovsky, D.G. Shaysultanov, N.D. Stepanov, A.V. Kuznetsov, I.V. Kolodiy, A.S. Tortika, O.N. Senkov, *J. Alloy Compd.* **591**, 11 (2014)
- H. Chen, A. Kauffmann, S. Laube, I.-C. Choi, R. Schwaiger, Y. Huang, K. Lichtenberg, F. Müller, B. Gorr, H.-J. Christ, M. Heilmaier, *Metall. Mater. Trans. A* **49**, 772 (2018)
- Y. Zhang, Y. Zhou, J. Lin, G. Chen, P. Liaw, *Adv. Eng. Mater.* **10**, 534 (2008)
- L. Jiang, Y. Lu, Y. Dong, T. Wang, Z. Cao, T. Li, *Appl. Phys. A* **119**, 291 (2015)

**Publisher's Note** Springer Nature remains neutral with regard to jurisdictional claims in published maps and institutional affiliations.